Published in final edited form as:

Langmuir. 2019 February 05; 35(5): 1379–1390. doi:10.1021/acs.langmuir.8b01597.

Engineering the surface properties of a zwitterionic polymer brush to enable simple fabrication of inkjet printed point-of-care immunoassays

Cassio M. Fontes[1,†], **Rohan K. Achar**[1,†], **Daniel Y. Joh**[1], **Imran Ozer**[1], **Somnath Bhattacharjee**[1], **Angus Hucknall**[1], **Ashutosh Chilkoti**[1,*]

[1]Department of Biomedical Engineering, Pratt School of Engineering, Duke University, Durham NC 27708 USA.

Abstract

Motivated by the lack of adventitious protein adsorption on zwitterionic polymer brushes that promise low noise and hence high analytical sensitivity for surface-based immunoassays, we explored their use as a substrate for immunoassay fabrication by inkjet printing of antibodies. We observed that a poly(sulfobetaine)methacrylate brush on glass is far too hydrophilic to enable non-covalent immobilization of antibodies by inkjet printing. To circumvent this limitation, we developed a series of hybrid zwitterionic-cationic surface coatings with tunable surface wettability that are suitable for inkjet printing of antibodies, but which also have low protein adsorption. We show that in a microarray format in which both capture and detection antibodies are discretely printed as spots on these hybrid brushes, a point-of-care sandwich immunoassay can be carried out with an analytical sensitivity and dynamic range that is similar to or better than the same assay fabricated on a PEG-like brush. We also show that the hybrid polymer brushes do not bind anti-PEG antibodies that are ubiquitous in human blood, which can be a problem with immunoassays fabricated on PEG-like coatings.

Keywords

Nanoscale; Nonfouling; Tunable Polymer brush; Inkjet Printing

[*]**Corresponding Author:** Ashutosh Chilkoti / Department of Biomedical Engineering, PO Box 90281, Duke University, Durham NC 27708-0281 / Tel: (919) 660-5373 / chilkoti@duke.edu.

[†]These authors contributed equally to this work.

Author Contributions: CMF and RKA are co-lead authors, who participated in experimental design, data collection, data analysis, manuscript drafting, table/figure creation, and manuscript revision. AH, DYJ and IO conducted experiments, analyzed data, and participated in manuscript drafting/revision. SB participated in experiments and manuscript drafting/revision in matters related to the PDMAEMA brush synthesis. AC is the Principal Investigator who directed the studies and drafted/revised the manuscript. All authors read and approved the final manuscript.

Competing Interests Statement: The underlying technology of the D4 was developed by Drs. Hucknall and Chilkoti, and acquired by Immucor Inc. (Norcross, GA) in 2014. All other authors declare no competing financial interests.

SUPPORTING INFORMATION

Schematics of D4 assay fabrication strategy on non-fouling coatings, graphic representation of the steps that encompass the execution of the D4 assay, spot morphology pre- and post-assay run and their dimensions, x-ray photoelectron spectra of all substrate generated in this work and D4 assay dose-response curves fabricated on all respective substrate are presented in supporting information.

1. INTRODUCTION

Protein adsorption is the first step when a biological fluid contacts a surface,[1] and it plays a critical —and typically undesirable— role in most *in-vitro* diagnostics (IVD) applications, as non-specific protein adsorption can severely compromise the analytical sensitivity of the assay. To overcome adventitious protein adsorption on a surface, several strategies have been devised to create protein-resistant coatings, such as the covalent conjugation of the "stealth" —protein-resistant— polymer, poly(ethylene glycol) (PEG) [2–3], the adsorption of PEG-based surfactants such as Pluronics® [4–5] onto surfaces, the electrostatic adsorption of PEG-functionalized polymers [6–7] and self-assembled monolayers (SAMs) on gold that present terminal oligoethylene glycol moieties [8–9]. However, none of these approaches, with the exception of OEG-SAMs, completely eliminate protein adsorption, but OEG-SAMs are restricted to gold and silver as the substrate.

Motivated by the need for a general methodology to create a protein-resistant coating on diverse substrates, we developed polymer brushes of poly(oligoethylene glycol methacrylate) (POEGMA) by surface-initiated atom transfer radical polymerization (SI-ATRP) from an ATRP initiator that is tethered to the surface. These surface coatings combine the ease of formation and high surface density of SAMs with the robustness and thickness of polymer films to generate brush-like structures that can be grown in situ on diverse materials —gold[10–11], glass[12], and plastics[13]. SI-ATRP of the OEGMA monomer yields a polymer coating whose thickness can be tuned in the 5–100 nm range. We have shown that conformal POEGMA coatings synthesized by this SI-ATRP with a thickness ≥ 10 nm exhibit exceptional protein and cell resistance, even when exposed to complex milieu samples such as whole blood, serum, and plasma[14].

We also demonstrated the utility of POEGMA brushes for clinical diagnostics by developing a direct immobilization process in which capture antibodies (Ab_c) are inkjet printed on a protein-resistant —nonfouling— brush of POEGMA on glass, followed by a mild desiccation step, which enables non-covalent functionalization of the POEGMA brush with a capture antibody; because we use inkjet printing, multiplexing the assay is trivial as it simply involves printing different spots with different capture antibodies, followed by a single drying step[15–16]. We then extended this fabrication approach to create a point-of-care format, the "D4" assay, where both capture and fluorophore-labeled detection antibodies (Ab_d) are printed on-chip to integrate all components required for a sandwich immunoassay in a user-friendly, point-of-care test (POCT) format[17].

Despite their utility in eliminating protein adsorption and cell adhesion, all PEG-based coatings, including POEGMA brushes, have some limitations in bioanalytical setting. First, PEG auto-oxidizes into reactive groups when exposed to oxygen and transition metal ions present in biologically relevant samples, which can potentially limit the shelf-life of the assay[18]. Second, recent reports have demonstrated that the ubiquitous use of PEG in consumer and food products have led to the widespread prevalence of circulating anti-PEG antibodies[19–22] that bind to PEG, and to POEGMA coatings with side-chains longer than three ethylene glycol repeats[23]. These anti-PEG Abs that directly bind to POEGMA brushes can interfere with a wide range of immunoassays.

These limitations led us to explore zwitterionic (ZI) polymer brushes, as they are reported to exhibit exceptional resistance to the non-specific adsorption of proteins and adherence of cells[24]. Although zwitterionic polymer brush-coated surfaces have been employed in immunodiagnostics by covalent conjugation of capture reagents[25] to surfaces, this strategy has several key limitations, such as the need to activate the surface for conjugation, followed by deactivation of the reactive moieties prior to use. Chemical coupling of capture reagents also makes multiplexing of the assay for different analytes more difficult because of the need for sequential coupling of different capture moieties to spatially defined areas of the substrate.

Building upon these results, this paper has two goals: (1) to explore whether inkjet printing is feasible —similar to POEGMA brushes— as a fabrication methodology for a POC microarray immunoassay on a non-fouling zwitterionic polymer brush; and to (2) to investigate the analytical performance of point-of-care microarrays printed on zwitterionic polymer brushes. We demonstrate that a commonly used “nonfouling” zwitterionic polymer brush, such as poly(sulfobetaine)methacrylate (PSBMA) does not have the required surface properties to enable non-covalent functionalization of antibodies by inkjet printing, as it is far too hydrophilic. To circumvent this limitation, we developed and characterized a series of new hybrid zwitterionic-cationic polymer brush coatings with tunable surface wettability that is suitable for inkjet printing of antibodies and show that a point-of-care microarray immunoassay fabricated on these hybrid brushes have a similar analytical sensitivity and dynamic range as those fabricated on POEGMA brushes. We also show that the mixed zwitterionic polymer brushes do not bind anti-PEG antibodies that are ubiquitous in human blood, which can be a problem with POEGMA brushes or other PEG-functionalized surface coatings.

2. EXPERIMENTAL SECTION

2.1. SI-ATRP of PSBMA, PDMAEMA and POEGMA on SiO_2 Surfaces

A. Functionalization of SiO_2 surfaces with ATRP initiator: Unless stated otherwise, all reagents were obtained from Sigma Aldrich (St. Louis, MO). Glass slides (Schott Nexterion® Glass B; Elmsford, NY) and silicon wafers with a thermally grown oxide layer (University Wafer, Inc; Boston, MA), were diced into 1×1 cm chips, and were then immersed in a 10% (v/v) solution of (3-aminopropyl)triethoxysilane (APTES) (Gelest, Inc.; Morrisville, PA) in ethanol (200-proof) for 4 h. The substrate were then extensively rinsed with ethanol and deionized (DI) water, centrifuged at 150 rcf on an Allegra X-15R Centrifuge (Beckman Coulter; Indianapolis, IN) for 6 min, and then cured overnight in an oven at 120°C. After cooling to room temperature, they were immersed in a solution of 1% (v/v) α-bromoisobutyryl bromide (BiB) and 1% (v/v) triethylamine in dichloromethane. Following incubation for 30 min, the substrate were removed from solution and consecutively rinsed with fresh dichloromethane, ethanol, and DI water. Finally, the substrate were centrifuged at 150 rcf on an Allegra X-15R Centrifuge (Beckman Coulter; Indianapolis, IN) for 6 min and cured in an oven at 120°C for 2 h, leading to surfaces functionalized with the ATRP initiator — BiB (“APTES-BiB”).

B. Preparation of sulfobetaine methacrylate (SBMA) solution for polymerization: Under an argon environment, a solution composed of 56 g of inhibitor-free SBMA, 1.49 g of copper (II) bromide, and 9.21 mL of 1,1,4,7,10,10-hexamethyltriethylenetetramine (HMTETA) was dissolved in 210 mL of methanol and 80 mL of DI water, and degassed by sparging with N_2 gas for 3 h. Next, 2.86 g of copper (I) bromide was slowly added to the solution under mild stirring until the salt was fully dissolved.

C. Preparation of 2-(Dimethylamino)ethyl methacrylate (DMAEMA) solution for polymerization: A solution composed of 150 g of DMAEMA (inhibitor-free), 28 mg of copper (II) bromide, 100 μL of HMTETA and 250 mL of DI was degassed by sparging with helium for 3 h.

D. Preparation of POEGMA solution for polymerization: A solution composed of 50 g POEGMA (inhibitor-free), 28 mg of copper (II) bromide, 100 μL of HMTETA and 350 mL of DI water was degassed by sparging with helium for 3 h.

E. Surface-initiated atom-transfer radical polymerization (SI-ATRP) of SBMA: Under an argon environment, the ATRP initiator-functionalized substrate (APTES-BiB) were incubated in the polymerization solution for a period of time which varied depending on the thickness required, (Figure 1B) and were then extensively rinsed with DI water. Finally, the substrate were spun dry for 6 min at 150 rcf on an Allegra X-15R Centrifuge (Beckman Coulter; Indianapolis, IN) and then stored under ambient conditions for subsequent use.

F. Surface-initiated activator regenerated by electron transfer atom-transfer radical polymerization (SI-ARGET-ATRP) of DMAEMA and POEGMA: Under an argon environment, 600 mg of sodium ascorbate were added to the polymerization solution previously described. The solution exhibited a color change from blue to violet, indicating reduction of Cu(II) cations to Cu(I) and the substrate were immersed in the polymerization solution for a specified time that varied depending upon the thickness of the polymer brush required (Figure 4B). Next, the substrate were extensively rinsed with DI water. Finally, the substrate were spun dry for 6 min at 150 rcf on an Allegra X-15R Centrifuge (Beckman Coulter; Indianapolis, IN) and then stored under ambient conditions for subsequent use.

G. Conversion of PDMAEMA to PCBMA polymer brushes: A 20 mM solution of iodoacetic acid in 1X PBS was prepared and adjusted to a pH between 5 and 8 by dropwise addition of a 1N NaOH solution. Next, the PDMAEMA-coated substrate were incubated at 45 or 75 °C under mild stirring. Following incubation, the substrate were rinsed with DI water, spun dry for 6 min at 150 rcf with an Allegra X-15R Centrifuge (Beckman Coulter; Indianapolis, IN) and then stored under ambient conditions for subsequent use.

2.2. Surface Characterization Techniques

A. Reflective Mode Ellipsometry: Film thickness was measured using an M-88 spectroscopic ellipsometer (J.A. Woollam Co; Lincoln, NE) at angles of 65°, 70°, and 75°

and wavelengths of 400 to 800 nm. To determine polymer brush thickness, a Cauchy model[26] with optical constants provided by the instrument's software was used to minimize the mean squared error between the measured value of thickness and the thickness predicted by the model.

B. X-ray Photoelectron Spectroscopy: All substrate were rinsed with PBS at pH 9 and dried under a stream of N_2 gas prior to being scanned. Data was acquired using an AXIS Ultra X-ray photoelectron spectrometer (Kratos Analytical, Inc., Chestnut Ridge, NJ). The spectrometer was operated at 15 kV and 10 mA with a monochromatic AlK_α x-rays (spot size: 700 × 400 μm). Survey scans were carried out with 15 sweeps, a pass energy of 160 eV, an energy step of 1 eV and a dwell time of 200 msec. High resolution scans were performed with 25 sweeps, a pass energy of 20 eV, an energy step of 0.1 eV and a dwell time of 269.7 msec. Operating pressure was ~1×10^{-8} torr. All spectral data were analyzed with CASA XPS software (Casa Software, Ltd.).

C. Drop Contact Angle Measurements: Advancing sessile drop contact angles were measured with a Rame-Hart model 100–00 goniometer (Succasunna, NJ). Images were acquired immediately after a drop of DI water was placed on the surfaces and contact angles were measured with the software Rame-Hart Drop Image Standard.

D. Protein Adsorption: Substrate were incubated for 24 h in a solution of bovine serum albumin (BSA) conjugated to fluorescein isothiocyanate (FITC-BSA) at a concentration of 10 mg/mL in phosphate-buffered saline (PBS). Following incubation, substrate were rinsed with a 0.1% Tween-20 (v/v) in PBS wash buffer three times with a BioTek ELx 5012 plate washer (Winooski, VT) programmed to perform an initial aspiration and add the washer buffer at the rate of 300 $\mu L.s^{-1}$, while simultaneously aspirating the buffer at a rate of 300 $\mu L.s^{-1}$ with a height of 4 mm, to generate a very mild stream of wash buffer to displace unbound material on the surface of the substrate. This was followed by centrifugation for 5 s at 4800 rpm on a C1303 Slide Spinner (Labnet International; Edison, NJ) to remove excess liquid. Substrate were then allowed to dry under ambient conditions. Fluorescence imaging was performed using an Axon Genepix 4400 tabletop scanner (Molecular Devices; LLC, Sunnyvale, CA) under constant imaging conditions (photomultiplier gain of 400 and excitation power of 100) and an excitation wavelength of 488 nm.

E. Anti-PEG Antibody Binding Assays: Substrate were incubated for 1 h in a 0.01 mg/mL solution of rabbit anti-PEG Abs (ThermoFisher; Waltham, MA) in heat-inactivated calf serum (VWR; Radnor, PA). After rinsing three times with 0.1% Tween-20 (v/v) in PBS with a BioTek ELx 5012 plate washer (Winooski, VT) programmed to perform an initial aspiration and add the washer buffer at the rate of 300 $\mu L.s^{-1}$, while simultaneously aspirating the buffer at a rate of 300 $\mu L.s^{-1}$ with a height of 4 mm, to generate a very mild stream of wash buffer to displace unbound material on the surface of the substrate, surfaces were then incubated for 1 h in a 2 μg/mL solution of AlexaFluor 647 labeled anti-rabbit secondary Ab (ThermoFisher; Waltham, MA) in PBS. Substrate were washed with 0.1% Tween-20 (v/v) in PBS, using the sampe protocol with the BioTek ELx 5012 plate washer (Winooski, VT) and spun dry at 4800 rpm on a C1303 Slide Spinner (Labnet International;

Edison, NJ) and imaged on an Axon Genepix 4400 tabletop slide scanner (Molecular Devices; Sunnyvale, CA) under constant imaging conditions (photomultiplier gain of 750 and excitation power of 100) and an excitation wavelength of 635 nm.

2.3. Immunoassay Fabrication and Performance Evaluation on Polymer Brushes

A. D4 immunoassay fabrication on polymer brush-coated surfaces: Lyophilized anti-IL-6 capture and detection Abs (R&D Systems; Minneapolis, MN) were reconstituted in sterile-filtered PBS to a final concentration of 1 mg/mL. Next, detection Abs were directly conjugated to AlexaFluor 647 (ThermoFisher; Waltham, MA) as instructed by the manufacturer, and trehalose was added to a final concentration of 1.0 % (w/v). Next, Ab_c and fluorescently labeled Ab_d were printed on the substrate with a sciFLEXARRAYER S11 spotter (Scienion; Berlin, Germany). Capture spots were printed in a central array with detection spots in close proximity, but still spatially separated from the central Ab_c by hundreds of microns as shown in Figure 3. After printing, the chips were left to dry, protected from light in a vacuum chamber lined with desiccant material for 12 h under a mild vacuum of −25 in. Hg.

B. Dose-response curves: Dose-response curves were generated by exposing D4 microarrays to calf serum spiked with recombinant human IL-6 (R&D Systems; Minneapolis, MN) at different concentrations for 60 min. Following incubation, the microarrays were rinsed three times with 0.1% Tween-20 (v/v) in PBS with a BioTek ELx 5012 plate washer (Winooski, VT) programmed to perform an initial aspiration and add the washer buffer at the rate of 300 $\mu L.s^{-1}$, while simultaneously aspirating the buffer at a rate of 300 $\mu L.s^{-1}$ with a height of 4 mm, to generate a very mild stream of wash buffer to displace unbound material on the surface of the substrate. Next, the susbtrate were spun dry with a C1303 Slide Spinner (Labnet International; Edison, NJ). Arrays were imaged and quantified with an Axon Genepix 4400 (Molecular Devices; Sunnyvale, CA) with a photomultiplier gain of 750 and excitation power of 100. Limit-of-blank (LoB) was calculated by measuring the mean fluorescence intensity (μ) and standard deviation (σ) from 9 blank samples and employing the definition $LoB = \mu_{blank} + 1.645\sigma_{blank}$. Limit-of-detection (LoD) was calculated using low concentration samples (LCS) by using the definition $LoD = LoB + 1.645\sigma_{LCS}$. Finally, the dynamic range (DR) was determined by the range of concentration from the LoD to the greatest concentration that had a fluorescent signal greater than 3σ of the next lowest concentration in the dilution series. All data was fit with a 5-parameter logistic curve using OriginPro 9.0 ($OriginL_{ab}$ Corp; Northhampton, MA).

C. Imaging D4 Assays on POEGMA and PSBMA surfaces: Capture and detection spots inkjet printed on the surface of PSBMA- and POEGMA-coated slides were imaged before addition of analyte on an Eclipse ME600 optical microscope (Nikon; Melville, NY) under 100X magnification in bright field imaging mode. Post-assay, the surfaces were imaged with an Axon Genepix 4400 (Molecular Devices; Sunnyvale, CA) with a photomultiplier gain of 750 and excitation power of 100. Spot size was calculated with the aid of the GenePix Pro 7 software (Molecular Devices; Sunnyvale, CA).

2.4 Statistical Analysis.

Statistical analysis was performed with the aid of GraphPad Prism version 6.01 (GraphPad Software, Inc; San Diego, CA). Student t-test, one-way ANOVA followed by Tukey's post-hoc multiple comparisons test, and two-way ANOVA followed by Sidak's post-hoc multiple comparison test were employed to evaluate the statistical significance of differences between groups. Specifically, Student t-test was used to evaluate the statistical significance of the water contact angles on PSBMA- and POEGMA-coated surfaces. One-way ANOVA followed by Tukey's post-hoc test was used to evaluate the statistical significance of protein adsorption, anti-PEG Ab binding and water contact angles between all surfaces. Two-way ANOVA followed by Sidak's post-hoc test was used to evaluate the statistical significance of differences in the thickness of polymer brushes derivatized under different reaction conditions of pH and temperature, and differences between the spot diameters of capture and detection reagents printed on POEGMA and PSBMA brush-coated surfaces.

3. RESULTS AND DISCUSSION

Initially, we sought to employ inkjet printing of capture (Ab_c) and detection antibodies (Ab_d) on ZI-polymer coated surfaces to create D4 assay chips, in a similar fashion to the fabrication strategy employed on POEGMA brush surfaces. To this end, we performed ATRP with sulfobetaine methacrylate (SBMA) on glass slides with a covalently immobilized ATRP initiator (APTES-BiB) to create a PSBMA brush. While SBMA and carboxybetaine methacrylate (CBMA) are monomers that have been used to create nonfouling zwitterionic polymer brushes, we selected SBMA as the monomer because of its commercial availability and low cost. A summary of the synthesis route of PSBMA brushes on glass is shown in Figure 1A, and employs SBMA as the monomer, a mixture of Cu(I) and Cu(II) transition metal catalysts and HMTETA as the ATRP ligand in a methanol/water cosolvent. With this approach, we were able to synthesize PSBMA films with tunable thickness by varying the polymerization time. Figure 1B shows the polymer brush thickness on SiO_2 as a function of polymerization time, measured by reflective mode ellipsometry in air, and shows that the thickness of PSBMA increases monotonically as a function of polymerization time, reaching ~40 nm in just under 16 h. Although effective in producing films with tunable thicknesses, the "classical" ATRP methodology used here has several undesired features, such as the need for high concentration of a transition metal catalyst, and an oxygen-free atmosphere to carry out the reaction[27–28]. An alternative route for this polymerization is the use of activators regenerated by electron transfer (ARGET) ATRP, which can be carried out in an aqueous environment, uses a low concentration of transition metals, and is oxygen tolerant, resulting in a more environmentally friendly process with a greatly reduced need for solution deoxygenation[29]. We hence attempted to carry out ARGET-ATRP of SBMA brushes. We discovered, however, that early termination occurs in ARGET-ATRP of SBMA, resulting in polymer brushes with thicknesses ranging 3 to 7 nm thickness (data not shown). Consequently, we abandoned this approach for the synthesis of PSBMA brushes, because our previous work on POEGMA brushes had shown that a polymer film thickness greater than ~10 nm is required for protein resistance[11].

Following PSBMA brush synthesis, we characterized the polymer-coated glass substrate. First, we performed X-ray photoelectron spectroscopy (XPS) to analyze the molecular composition of the initiator and PSBMA-functionalized substrate. Figure 1C shows the survey scan spectrum of SiO_2 after functionalization with APTES-BiB, but prior to ATRP, which exhibits characteristic peaks associated with the SiO_2 substrate, and a small nitrogen peak at ~399 eV that can be attributed to the nitrogen moiety in the surface immobilized APTES. Figures 1D–E show survey scan spectra of 11 nm and 33 nm thick PSBMA brushes, where the insets depict high-resolution scans for the N_{1s} peak. As reported elsewhere, the bromide peak was not visible in the survey scan spectra[30]. Survey scans of the PSBMA brush-coated surfaces show large nitrogen and sulfur peaks, as expected from the composition of the polymer. The 11 nm thick PSBMA coating has small Si peaks, which is absent in the survey scan spectrum of the 33 nm PSBMA coating, a result consistent with the ~10 nm sampling depth of XPS [31]. High-resolution scans of 11 nm thick PSBMA coatings show a dominant quaternary (402.0 eV) amine peak originating from the polymer coating and a small tertiary (398.6 eV) peak associated with the underlying APTES-BiB layer. This latter peak is not detected with 33 nm brushes, further corroborating the results obtained from their survey scan spectra.

We next investigated the protein resistance of each PSBMA-modified surface and controls. To do so, bare glass, glass slides functionalized with APTES-BiB, and glass with ~40 nm thick POEGMA and PSBMA polymer brushes grafted from the surface were incubated in a solution of 10 mg/mL FITC-BSA in PBS for 24 h at room temperature. Following incubation, and a wash step with PBS and Tween-20 to remove unbound protein, the surfaces were imaged with a fluorescent slide scanner; the fluorescence intensity from the FITC channel is indicative of adsorption BSA on to the surface. Figure 2A shows a low fluorescence intensity of surfaces coated with POEGMA and PSBMA polymer brushes and a much higher fluorescence on APTES and APTES-BiB-functionalized substrate. These results quantified in Figure 2B and analyzed by one-way ANOVA followed by a post-hoc Tukey's test shows that protein adsorption on APTES-BiB and the APTES- functionalized surfaces are statistically significantly different from the PSBMA and POEGMA brush-coated surfaces and from glass ($p<0.001$). There was no statistically significant difference between APTES and APTES-BiB nor between glass, POEGMA and PSBMA. POEGMA-coated surfaces showed a slightly lower fluorescence than PSBMA, but this effect is not statistically significant, which corroborates a previous study [32].

Next, we sought to demonstrate that PSBMA brushes are not reactive towards anti-PEG Abs. We incubated PSBMA- and POEGMA-coated glass slides with rabbit anti-PEG polyclonal Abs for 1 h, rinsed the surfaces with 0.1% Tween-20 (v/v) in PBS, and then incubated with an AlexaFluor 647 labeled anti-rabbit secondary Ab in PBS for 1 h. We also incubated a POEGMA-coated glass slide with only a fluorescently labelled anti-rabbit Ab as a control for the effect of nonspecific binding of the detection antibody that is labeled $POEGMA_{(c)}$ in Figure 2D. Following a final wash with 0.1% Tween-20 (v/v) in PBS, the substrate were spun-dry and imaged with a slide scanner to detect AlexaFluor 647 fluorescence. Figure 2C shows the level of fluorescence on the POEGMA and PSBMA surfaces. In contrast to the PSBMA coating on glass, which shows a low level of fluorescence, the fluorescence emission levels from the POEGMA coated glass slide saturate

the detector, as seen by the white color in the fluorescence image, due to the high level of binding of the PEG side chains by the anti-PEG primary Ab (Figure 2C).

We quantified the fluorescence intensities from these images, and a one-way ANOVA analysis of the data, followed by a Tukey's post-hoc test shows that the binding of anti-PEG Ab on POEGMA-coated glass is statistically significantly different than on PSBMA coated glass, and from $POEGMA_{(c)}$, the negative control ($p < 0.0001$) (Figure 2D). In contrast, the fluorescence intensity from PSBMA coated glass was not statistically significantly different from the negative control, $POEGMA_{(c)}$.

After demonstrating the lack of protein adsorption and anti-PEG binding on the PSBMA coated glass, we fabricated D4 assays for the detection of IL-6 on POEGMA- and PSBMA-coated glass slides. As reported elsewhere in greater detail[17] and depicted in Figure S1A, we spotted an Ab_c for IL-6 in the central region of the chip and AlexaFluor647 labeled Ab_d in concentric patterns around the capture spots of Ab_c. Next, we ran the D4 assay by adding calf serum spiked with IL-6 to the chip surface (see Figure S1B). Figure 3A shows a representative D4 chip on POEGMA with the inkjet-printed Ab_c, PBS, and Ab_d spots spatially separated on the chip's surface, and shows the low background signal and high signal to noise ratio (S/N) obtained after incubation with calf serum spiked with IL-6 at a 3.9 ng/mL IL-6 concentration. Figure 3B shows the respective dose-response curve obtained for the detection of IL-6, and demonstrates the exceptional performance of this assay fabricated on the POEGMA-coated surfaces with a LOD of 26 pg/mL and dynamic range of 3.4.

Figure 3C shows a D4 chip for IL-6 fabricated on PSBMA brushes. In contrast to the POEGMA-coated surface, the capture spots are barely visible after completion of the IL-6 assay, and the detection spots have a much lower intensity and larger diameter than those on POEGMA. Furthermore, quantification of the data of PSBMA coated chips exposed to varying concentrations of IL-6 to create a dose-response curve for IL-6 shows that inkjet printing of the Ab_c and Ab_d does not yield a usable assay (Figure 3D). The spot morphology and low intensity of capture spots on the PSBMA surface when compared to POEGMA suggests that the failure of the D4 assay on the PSBMA-coated surface can be attributed to to its hydrophilicity (Figure S2A) and the consequent lack of stable Ab_c entrapment in the polymer brush.

To test this hypothesis, we next measured the water contact angles in air for POEGMA- and PSBMA-coated glass slides by the sessile drop technique (Figure 3E). The contact angle of the PSBMA-coated surface is ~8°, as compared to ~44° for the POEGMA-coated surface (Figure 3F), clearly showing that the PSBMA-coated surface is far more hydrophilic than POEGMA. A Student t-test of the contact angles reported in Figure 3F confirms that the difference between these contact angles is statistically significant ($p < 0.001$).

The extremely low contact angle of the PSBMA coated surface leads to spot sizes of ~300 μm for the Ab_c and Ab_d on PSBMA that are statistically different than the ~180 μm spot size on POEGMA (ANOVA followed by Sidak's post-hoc test, $p < 0.0001$). The greater hydrophilicity of PSBMA, results in a larger spot size than on POEGMA and also suggests a much lower level of Ab_c entrapment in the zwitterionic polymer brush coated surfaces.

These results show that inkjet printing of Ab_c and Ab_d for fabrication of immunodiagnostics is not feasible with these extremely hydrophilic polymer coatings.

To solve the inkjet printing problem on the PSBMA surface —and potentially on other highly hydrophilic ZI polymer coatings— we next developed a new route to synthesize tunable “hybrid” polymer brushes that present a protein-resistant zwitterionic side-chain on a polymer backbone, but that would also enable inkjet printing. This approach involves the synthesis of a hybrid polymer brush that contains ZI and amine groups, that we hypothesized would allow immobilization of proteins via inkjet printing due to electrostatic and hydrogen bonding with antibodies but also present a sufficiently high concentration of ZI side-chains to provide protein resistance in the regions not printed with the assay reagents.

Figure 4A depicts the synthesis strategy that we used to implement this approach, where poly-2-(dimethylamino)ethyl methacrylate (PDMAEMA) brushes with amine groups in the side chains are grafted from the surface by ARGET-ATRP, and are then reacted with iodoacetic acid under different conditions of pH and temperature to generate PCBMA-PDMAEMA hybrid brushes with different fractions of amine-terminated and ZI CBMA side-chains. We hypothesized that a higher pH and temperature of the derivatization reaction would yield higher degrees of conversion of the amine into zwitterionic CBMA groups so that temperature and pH could be used to tune the degree of conversion of the amine groups into CBMA moieties and thereby tune the protein chemistry to enable inkjet printing of Abs into the polymer brush without sacrificing its protein resistance.

To explore this approach, we first systematically varied the polymerization time of PDMAEMA on APTES-BiB-functionalized glass slides and SiO_2 chips, thereby obtaining PDMAEMA brushes of different thicknesses, as measured by ellipsometry (Figure 4B). After the PDMAEMA brushes were synthesized, we sought to control the extent of conversion of PDMAEMA to PCBMA by derivatizing the PDMAEMA-coated surfaces with 20 mM iodoacetic acid solution at a range from pH 5–8 and at 45 or 75°C for 24 h. Following derivatization, we measured the polymer brush thickness by ellipsometry and compared those values with their thickness prior conversion. Figure 4C shows that following derivatization, the brushes show a statistically significant increase in brush thickness. Two-way ANOVA comparison of measured values (data in Figure 2C) followed by Sidak’s post-hoc test indicates that all differences in thickness pre-and post-conversion are statistically significant ($p < 0.001$). The origin for the increase in thickness is not entirely clear but we speculate they may rise from a combination of factors: (1) the additional mass added to the side chains by derivatization of the amine group, (2) the increase in the side chains charge, which we speculate possibly increases the water retention —even in the macroscopically dry state that ellipsometry is carried out in—and consequently brush volume; and (3) a change in conformation of the polymer brush to a more stretched conformation. Elucidation of the precise cause of this change, is however, beyond the scope of this study.

Next, we performed XPS on ~40 nm thick PDMAEMA and mixed PCBMA-PDMAEMA brushes, as measured by ellipsometry in air. Figure 5A shows the survey scan spectrum of the PDMAEMA brush, where characteristic peaks for C_{1s}, N_{1s} and O_{1s} can be identified, consistent with the composition of the polymer. The inset in Figure 5A shows a high-

resolution N_{1s} spectrum of the PDMAEMA brush, and peak fitting showed that it could be fit with a single component that can be assigned to tertiary amines (398.6 eV), which is consistent with the chemical structure of PDMAEMA. Figures 5B–E show the high-resolution N_{1s} spectra of PDMAEMA derivatized with iodoacetic acid at different combinations of temperature and pH. The peak fits of the high-resolution scans are instructive, as they show that depending upon the specific derivatization conditions, a significant fraction of the tertiary amines (398.6 eV) are converted into quaternary (402.0 eV) amines that are a signature of PCBMA. Table 1 (and Figure S3) show the quantified XPS data, and reveal that at both 45 °C and 75 °C, the yield of the derivatization reaction shows a maximum at pH 7, leading to the conversion of up to two-thirds of the tertiary amines into quaternary amines that are indicative of PCBMA.

Following XPS analysis, we measured the protein adsorption, water contact angle, and anti-PEG Ab binding on PDMAEMA, and ZI hybrid surfaces. Figure 6A shows fluorescence images of these surfaces after incubation with FITC-BSA, the intensity of which is reflective of the level of adsorption of the protein on these coatings. These intensities were quantified and analyzed by one-way ANOVA followed by Tukey's post-hoc test, which shows a statistically significant difference between the groups at $p<0.001$ level (Figure 6B).

PDMAEMA has a high level of protein adsorption, which can be attributed to its highly charged surface that electrostatically binds proteins. Interestingly, iodoacetic acid derivatization at pH 5, 45°C caused a statistically significant increase in protein absorption when compared to PDMAEMA coatings, which was not expected as the insertion of zwitterionic chemical motifs should increase protein resistance. However, as the temperature and pH of the derivatization reaction increases, the surfaces become more protein resistant, a trend that is clearly seen in Figure 6B and is consistent with increasing conversion of the amine group to zwitterions (Figure 5 and Table 1). The derivatized surfaces labeled A-F in Figure 6B have protein resistance levels that are comparable to those of PSBMA but are all somewhat higher than POEGMA.

We next measured the sessile water contact angle on these surfaces. Figure 7A shows photographs of water drops on different surfaces, and Figure 7B shows the water contact angles on all polymer coated substrate. One-way ANOVA analysis followed by a Tukey's post-hoc test indicates statistically significant differences amongst the groups ($p<0.001$). These results clearly demonstrate that a higher degree of surface derivatization yields more hydrophilic surfaces. These results are consistent with the protein resistance assays and XPS data, as there is a near monotonic increase in protein resistance and reduction in water drop contact angle as the fraction of zwitterionic groups increases. Furthermore, XPS analysis showed that pH 8 at 75°C presented lower derivatization ratios than pH 7 at 75°C. These findings correlate directly to a larger water drop contact angle and although the non-specific protein binding measurements for substrate converted under pH 8 75°C are smaller than those of pH 7 75°C, this difference is not statistically significant. These results clearly demonstrate that there is a direct dependency between the degree of zwitterionic groups on the substrate and surface hydrophilicity and a somewhat weaker trend with respect to protein resistance. The one exception to this trend is POEGMA, which has the lowest protein adsorption, but has a significantly higher water contact angle of ~44°. These results clearly

indicate that although hydrophilicity is important for protein resistance it is not its sole determinant, results which are consistent with a substantial body of literature on this topic[33–38].

Next, we examined the binding of an anti-PEG Ab to these surfaces. As the derivatized polymer brushes do not present ethylene glycol chains in their structure, the binding of anti-PEG and the fluorescently labelled secondary Ab can be attributed to non-specific adsorption rather than molecular recognition of the brushes' side-chain by the anti-PEG primary antibodies, as is the case with POEGMA coatings. As shown in Figure 8A, the fluorescence intensity reduces with the increase in pH and temperature at which the derivatization reaction was carried out. One-way ANOVA with Tukey's post-hoc test comparing the measurements performed on all substrates shows that the difference in fluorescence between the majority of the substrate is statistically significant at a $p<0.001$ significance level. The lowest non-specific adsorption of anti-PEG observed on iodoacetic acid-derivatized PDMAEMA brushes required either a high pH of 8 or a high temperature of 75°C. Anti-PEG adsorption on these derivatized surfaces were statistically indistinguishable from that on the PSBMA brush.

Finally, we sought to correlate surface properties with D4 assay performance fabricated on these substrate. The immunoassay fabrication on the PCBMA-PDMAEMA brushes followed the same methodology, as depicted in Figure S1A. Dose-response curves were obtained for each substrate by incubating 80 μL of analyte-spiked IL-6 calf serum for 1 h followed by a rinse in 0.1% Tween-20 (v/v) in PBS and imaging on a fluorescence slide scanner. Figure 9A shows the results of a D4 assay on virgin PDMAEMA brushes, with fluorescence images in each panel depicting the raw readout of each assay. The high level of non-specific adsorption, visible by the red fluorescence throughout the chip surface drowns out the signal from the printed spots of the Ab_c, making it impossible to construct a dose-response curve.

Figure 9B shows the dose-response curve of a PDMAEMA substrate derivated at 45°C and pH 5. As can be seen in the fluorescence image of the chip, the background fluorescence caused by non-specific binding is significantly lower than for native PDMAEMA chip (Figure 9A), so that the capture spots are clearly visible against the background, enabling a dose response-curve to be generated, albeit with a fairly high baseline. Figure 9C shows that when the pH is held constant at 5, but the temperature of the derivatization reaction is increased to 75°C, the surface becomes protein-resistant to a degree that allows a dose-response curve to be determined. We can clearly see that the background signal on this inset is low and that the capture spots can be clearly resolved. Figures 9D–E presents the dose-response behavior obtained with other conditions, and Figure S4 depicts all dose-response curves generated in this work. Table 2 presents the figures of merit (FOM) calculated by averaging 4 independently determined dose-response curves and correlates these FOMs with water contact angle (WTCA) and surface protein absorbance, measured by fluorescence intensity.

As can be seen by the results presented in Table 2, we were able to control protein resistance and hydrophilicity by gradually increasing the proportion of zwitterionic groups on a

PDMAEMA polymer brush. This allowed us to reach LODs close to those obtained on POEGMA coatings, the gold standard of surface coatings for protein microarray applications. Furthermore, we were able to obtain DRs that were somewhat greater than obtained on POEGMA, most likely due to the higher density of Ab_c immobilized in the capture spots. It should also be noted that we can tune the surface properties by controlling the degree of polymer brush derivatization, which can be used to yield optimized surfaces for protein microarray applications. We hypothesize that non-covalent surface functionalization for IVD applications requires a surface to present a fine balance between protein resistance and surface hydrophilicity (which POEGMA naturally presents). This becomes clear when analyzing the PDMAEMA-PCBMA surfaces that yielded the lowest LODs and largest DRs and comparing with POEGMA- and PSBMA-coated surfaces. These hybrid substrate present moderate levels of protein resistance and intermediate values of water drop contact angles. Other surfaces with very high non-specific protein binding capabilities have the capture spot signal drowned by the background noise such as PDMAEMA and PDMAEMA-PCBMA pH 5 45°C. On the other end of the spectrum, substrate with low fouling levels and small water drop contact angles, such a PSBMA-coated surfaces, which entail elevated levels of hydrophilicity, also present less than optimal characteristics for non-covalent surface biofunctionalization.

4. CONCLUSIONS

The D4 assay is a self-contained point of care test (POCT) format based on the sandwich immunoassay. Manufacturing the assay requires inkjet printing of capture and detection antibodies in separate spots on a surface. The surface must however also be protein resistant in its wet, hydrated state during the assay, so as to allow testing from blood or other complex biological fluids. Motivated by reports of the protein resistance of zwitterionic polymers brushes, we explored their use for fabrication of the D4-POCT. We found that although PSBMA zwitterionic brushes are nonfouling in their hydrated state, consistent with previous reports, they were unsuitable as a substrate for inkjet printing of antibodies in the dry state, as they are too wettable.

These results inspired us to develop a hybrid zwitterionic brush that would enable inkjet printing of antibodies in its dry state, yet retain good protein resistance in its hydrated state. To do so, we developed a 2-step synthesis where an amine-functionalized brush of PDMAEMA is grown from the surface by ATRP, followed by chemical derivatization of a fraction of the amine groups to generate a hybrid PCBMA-PDMAEMA brush. By controlling the extent of derivatization of the amine group to a carboxybetaine moiety, we created surfaces that satisfy both requirements. The hybrid polymer brushes were tested for detection of IL-6 in a D4-POCT, and showed analytical figures-of-merit that are comparable to the same assay fabricated on a POEGMA brush, with the added advantage that they do not cross-react with anti-PEG antibodies that are ubiquitous in human blood and that can compromise the utility of the D4-POCT on a POEGMA brush surface. This synthesis strategy provides a new class of polymer coatings for inkjet printed point-of-care protein microarrays that exhibit a low detection limit and a high dynamic range.

Supplementary Material

Refer to Web version on PubMed Central for supplementary material.

ACKNOWLEDGMENTS

The authors acknowledge funding from the United States Special Operations Command, contract number W81XWH-16-C-0219 and the Combat Casualty Care Research Program (JPC-6) contract number W81XWH-17–2-0045. CMF also acknowledges the financial support from the National Council for the Improvement of Higher Education - CAPES (the Science without Borders Project).

REFERENCES

1. Rabe M; Verdes D; Seeger S, Understanding protein adsorption phenomena at solid surfaces. Advances in colloid and interface science 2011, 162 (1–2), 87–106. [PubMed: 21295764]
2. Amiji M; Park K, Surface modification of polymeric biomaterials with poly(ethylene oxide), albumin, and heparin for reduced thrombogenicity. Journal of Biomaterials Science, Polymer Edition 1993, 4 (3), 217–234. [PubMed: 8476792]
3. Zhang M; Desai T; Ferrari M, Proteins and cells on PEG immobilized silicon surfaces. Biomaterials 1998, 19 (10), 953–960. [PubMed: 9690837]
4. Li J-T; Caldwell KD; Rapoport N, Surface properties of pluronic-coated polymeric colloids. Langmuir 1994, 10 (12), 4475–4482.
5. Wu MH, Simple poly(dimethylsiloxane) surface modification to control cell adhesion. Surface and Interface Analysis 2009, 41 (1), 11–16.
6. Tosatti S; Paul SMD; Askendal A; VandeVondele S; Hubbell JA; Tengvall P; Textor M, Peptide functionalized poly(l-lysine)-g-poly(ethylene glycol) on titanium: resistance to protein adsorption in full heparinized human blood plasma. Biomaterials 2003, 24 (27), 4949–4958. [PubMed: 14559008]
7. Marie R; Beech JP; Vörös J; Tegenfeldt JO; Höök F, Use of PLL-g-PEG in micro-fluidic devices for localizing selective and specific protein binding. Langmuir 2006, 22 (24), 10103–10108. [PubMed: 17107006]
8. Prime KL; Whitesides GM, Adsorption of proteins onto surfaces containing end-attached oligo(ethylene oxide): a model system using self-assembled monolayers. Journal of the American Chemical Society 1993, 115 (23), 10714–10721.
9. Ostuni E; Yan L; Whitesides GM, The interaction of proteins and cells with self-assembled monolayers of alkanethiolates on gold and silver. Colloids and Surfaces B: Biointerfaces 1999, 15 (1), 3–30.
10. Ma H; Hyun J; Stiller P; Chilkoti A, “Non-Fouling” oligo(ethylene glycol)- functionalized polymer brushes synthesized by surface-initiated atom transfer radical polymerization. Advanced Materials 2004, 16 (4), 338–341.
11. Ma H; Wells M; Beebe TP; Chilkoti A, Surface-initiated atom transfer radical polymerization of oligo(ethylene glycol) methyl methacrylate from a mixed self-assembled monolayer on gold. Advanced Functional Materials 2006, 16 (5), 640–648.
12. Ma H; Li D; Sheng X; Zhao B; Chilkoti A, Protein-resistant polymer coatings on silicon oxide by surface-initiated atom transfer radical polymerization. Langmuir 2006, 22 (8), 3751–3756. [PubMed: 16584252]
13. Hucknall A; Simnick AJ; Hill RT; Chilkoti A; Garcia A; Johannes MS; Clark RL; Zauscher S; Ratner BD, Versatile synthesis and micropatterning of nonfouling polymer brushes on the wafer scale. Biointerphases 2009, 4 (2), FA50–FA57. [PubMed: 20408717]
14. Thevenot P; Hu W; Tang L, Surface chemistry influence implant biocompatibility. Current topics in medicinal chemistry 2008, 8 (4), 270–280. [PubMed: 18393890]
15. Hucknall A; Kim D-H; Rangarajan S; Hill RT; Reichert WM; Chilkoti A, Simple fabrication of antibody microarrays on nonfouling polymer brushes with femtomolar sensitivity for protein analytes in serum and blood. Advanced Materials 2009, 21 (19), 1968–1971. [PubMed: 31097880]

16. Hucknall A; Rangarajan S; Chilkoti A, In Pursuit of Zero: Polymer brushes that resist the adsorption of proteins. Advanced Materials 2009, 21 (23), 2441–2446.
17. Joh DY; Hucknall AM; Wei Q; Mason KA; Lund ML; Fontes CM; Hill RT; Blair R; Zimmers Z; Achar RK; Tseng D; Gordan R; Freemark M; Ozcan A; Chilkoti A, Inkjet-printed point-of-care immunoassay on a nanoscale polymer brush enables subpicomolar detection of analytes in blood. Proceedings of the National Academy of Sciences 2017.
18. Lyu S; Untereker D, Degradability of Polymers for Implantable Biomedical Devices. International Journal of Molecular Sciences 2009, 10 (9), 4033–4065. [PubMed: 19865531]
19. Ganson NJ; Povsic TJ; Sullenger BA; Alexander JH; Zelenkofske SL; Sailstad JM; Rusconi CP; Hershfield MS, Pre-existing anti–polyethylene glycol antibody linked to first-exposure allergic reactions to pegnivacogin, a PEGylated RNA aptamer. Journal of Allergy and Clinical Immunology 2016, 137 (5), 1610–1613.e7. [PubMed: 26688515]
20. Lubich C; Allacher P; de la Rosa M; Bauer A; Prenninger T; Horling FM; Siekmann J; Oldenburg J; Scheiflinger F; Reipert BM, The mystery of antibodies against polyethylene glycol (PEG) - What do we know? Pharmaceutical research 2016, 33 (9), 2239–49. [PubMed: 27271335]
21. Yang Q; Jacobs TM; McCallen JD; Moore DT; Huckaby JT; Edelstein JN; Lai SK, Analysis of pre-existing IgG and IgM antibodies against polyethylene glycol (peg) in the general population. Analytical Chemistry 2016, 88 (23), 11804–11812. [PubMed: 27804292]
22. Chen B-M; Su Y-C; Chang C-J; Burnouf P-A; Chuang K-H; Chen C-H; Cheng T-L; Chen Y-T; Wu J-Y; Roffler SR, Measurement of pre-existing IgG and IgM antibodies against polyethylene glycol in healthy individuals. Analytical Chemistry 2016, 88 (21), 10661–10666. [PubMed: 27726379]
23. Qi Y; Simakova A; Ganson NJ; Li X; Luginbuhl KM; Ozer I; Liu W; Hershfield MS; Matyjaszewski K; Chilkoti A, A brush-polymer/exendin-4 conjugate reduces blood glucose levels for up to five days and eliminates poly(ethylene glycol) antigenicity. Nature Biomedical Engineering 2016, 1, 0002.
24. Rodriguez-Emmenegger C; Kylián O; Houska M; Brynda E; Artemenko A; Kousal J; Alles AB; Biederman H, Substrate-independent approach for the generation of functional protein resistant surfaces. Biomacromolecules 2011, 12 (4), 1058–1066. [PubMed: 21381652]
25. Vaisocherová H; Yang W; Zhang Z; Cao Z; Cheng G; Piliarik M; Homola J; Jiang S, Ultralow fouling and functionalizable surface chemistry based on a zwitterionic polymer enabling sensitive and specific protein detection in undiluted blood plasma. Analytical Chemistry 2008, 80 (20), 7894–7901. [PubMed: 18808152]
26. Gupta Y; Arun P, First Step to Ellipsometry. International Journal of Physics 2015, 3 (1), 8–11.
27. Matyjaszewski K, Atom transfer radical polymerization (ATRP): Current status and future perspectives. Macromolecules 2012, 45 (10), 4015–4039.
28. Matyjaszewski K, Atom transfer radical polymerization: from mechanisms to applications. Israel Journal of Chemistry 2012, 52 (3–4), 206–220.
29. Simakova A; Averick SE; Konkolewicz D; Matyjaszewski K, Aqueous ARGET ATRP. Macromolecules 2012, 45 (16), 6371–6379.
30. Joh DY; McGuire F; Abedini-Nassab R; Andrews JB; Achar RK; Zimmers Z; Mozhdehi D; Blair R; Albarghouthi F; Oles W; Richter J; Fontes CM; Hucknall AM; Yellen BB; Franklin AD; Chilkoti A, Poly(oligo(ethylene glycol) methyl ether methacrylate) brushes on high-kappa metal oxide dielectric surfaces for bioelectrical environments. ACS applied materials & interfaces 2017, 9 (6), 5522–5529. [PubMed: 28117566]
31. Matthew, J., Surface analysis by Auger and X-ray photoelectron spectroscopy. D. Briggs and J. T. Grant (eds). IMPublications, Chichester, UK and SurfaceSpectra, Manchester, UK, 2003. 900 pp., ISBN 1-901019-04-7, 900 pp. Surface and Interface Analysis 2004, 36 (13), 1647–1647.
32. Ladd J; Zhang Z; Chen S; Hower JC; Jiang S, Zwitterionic polymers exhibiting high resistance to nonspecific protein adsorption from human serum and plasma. Biomacromolecules 2008, 9 (5), 1357–1361. [PubMed: 18376858]
33. Lenk TJ; Horbett TA; Ratner BD; Chittur KK, Infrared spectroscopic studies of time-dependent changes in fibrinogen adsorbed to polyurethanes. Langmuir 1991, 7 (8), 1755–1764.
34. Shen M; Martinson L; Wagner MS; Castner DG; Ratner BD; Horbett TA, PEO-like plasma polymerized tetraglyme surface interactions with leukocytes and proteins: in vitro and in vivo

studies. Journal of biomaterials science. Polymer edition 2002, 13 (4), 367–90. [PubMed: 12160299]

35. Horbett TA; Brash JL, Proteins at Interfaces II American Chemical Society: 1995; Vol. 602, p 580.
36. Llanos GR; Sefton MV, Immobilization of poly(ethylene glycol) onto a poly(vinyl alcohol) hydrogel: 2. Evaluation of thrombogenicity. Journal of Biomedical Materials Research 1993, 27 (11), 1383–1391. [PubMed: 8263000]
37. Vogler EA, Protein adsorption in three dimensions. Biomaterials 2012, 33 (5), 1201–1237. [PubMed: 22088888]
38. Chen S; Li L; Zhao C; Zheng J, Surface hydration: Principles and applications toward low-fouling/nonfouling biomaterials. Polymer 2010, 51 (23), 5283–5293.

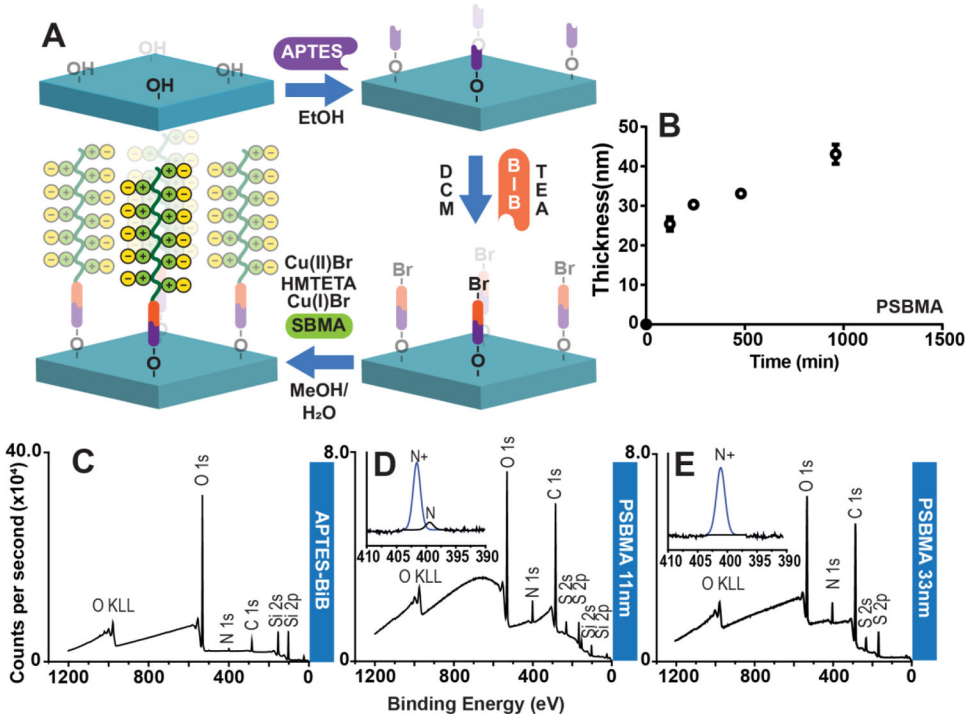

Figure 1: Polymer brushes brushes grown from silicon oxide and glass substrate and XPS characterization of substrate.

(A) Representative stepwise strategy of PSBMA brush synthesis on thermally-deposited SiO_2 on Si, and on glass slides. Surface functionalization with APTES allows installation of ATRP initiator, BiB (α-bromoisobutyryl bromide). PSBMA brushes are then "grafted from" the surface by ATRP. **(B)** PSBMA brush growth on SiO_2 at the indicated timepoints was investigated by reflective mode ellipsometry. Each data point is the average of three independent replicates. **(C)** XPS survey scan spectrum of APTES-BiB (initiator) covalently attached to SiO_2 surface. **(D)** XPS survey scan spectrum of 11 nm thick PSBMA coating shows reduction in intensity O_{1s} and Si_{2s} and Si_{2p} peaks, an increase in the intensity of the N_{1s} peak compared to the APTES-BiB modified glass surface,and the appearence of S_{2s} and S_{2p} peaks that are consistent with formation of a PSBMA overlayer. Inset: High resolution N_{1s} spectrum of PSBMA with peak fitting, showing the prevalence a component peak corresponding to quaternary amine that is consistent with the chemical structure of PSBMA, and a smaller component peak corresponding to tertiary amine groups from the APTES-BiB underlayer. **(E)** Survey scan spectrum of 33 nm thick PSBMA coating on glass shows characteristic S_{2s} and S_{2p} from the PSBMA overlayer and the absence of silicon peaks, consistent with the PSMA overlayer that is greater than the sampling depth of XPS. Inset: High resolution N_{1s} spectrum with peak fitting following ATRP, showing the prevalence of quaternary amines consistent with formation of a PSBMA overlayer. Abbreviations: H_2O = water, EtOH = ethanol, MeOH = methanol, DCM = dichloromethane, TEA = triethylamine, Cu(I)Br = copper I bromide; Cu(II)Br = copper II bromide; HMTETA = 1,1,4,7,10,10-Hexamethyltriethylenetetramine, SA = sodium ascorbate, SBMA = sulfobetaine methacrylate, CBMA = carboxibetaine methacrylate, N = tertiary amines, N+ = quaternary amines.

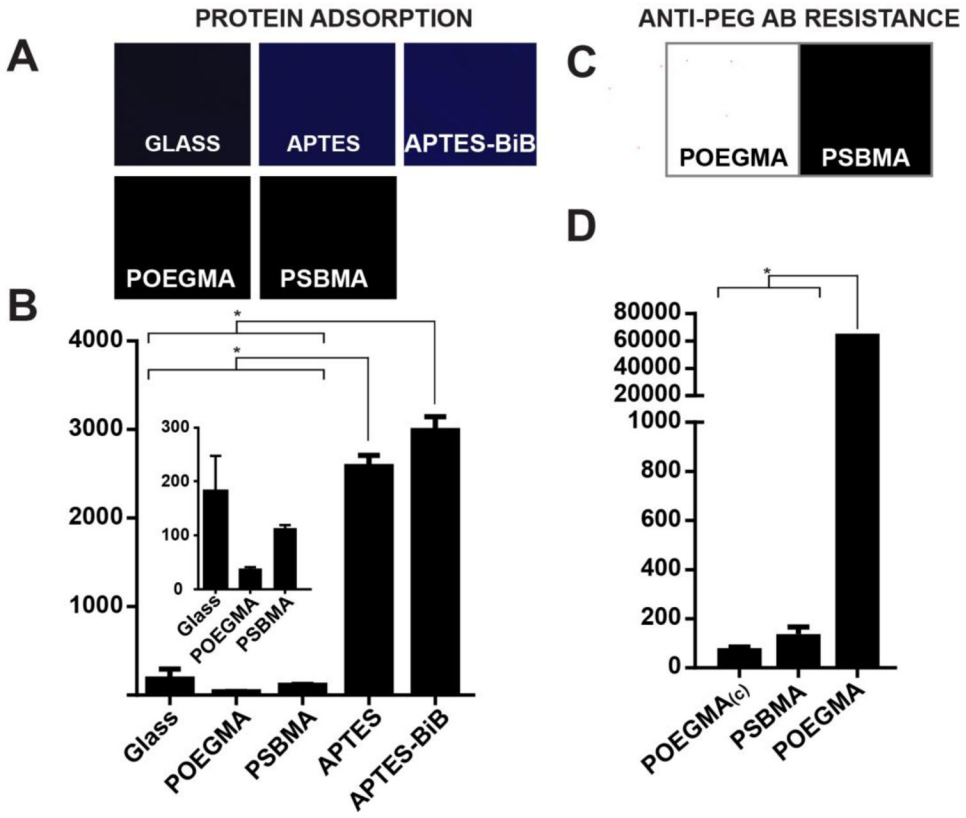

Figure 2: Protein adsorption and anti-PEG Ab binding on POEGMA and PSBMA brushes.

(A) Fluorescence images and **(B)** quantification of adsorption of FITC-BSA (10mg/mL in PBS) on glass, APTES and APTES-BiB functionalized glass and POEGMA and PSBMA brushes. There is a statistically significant difference between group means as determined by one-way ANOVA followed by Tukey's post-hoc test ($p<0.001$). Means with lines between bars and marked with a * are significantly different. **(C)** Fluorescence images and **(D)** quantification of anti-PEG Ab binding on POEGMA and PSBMA. There is a statistically signicant difference between group means as determined by one-way ANOVA followed by Tukey's post-hoc test ($p<0.001$). Means with lines between bars and marked with a * are significantly different.

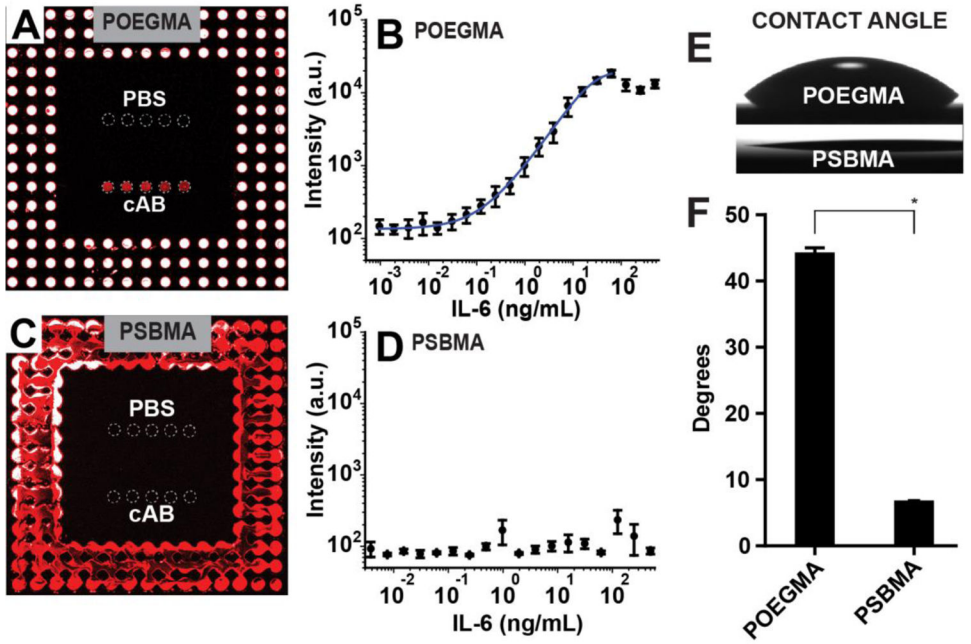

Figure 3: D4 assay on POEGMA and PSBMA brushes.

(A and C) Fluorescence images and dose-response curves **(B and D)** of D4 microarrays against IL-6 fabricated on POEGMA (A-B) and PSBMA (C-D) brushes. Alexafluor 647 conjugated detection antibodies are spotted around unlabelled capture antibody and phosphate buffered saline (PBS) spots (negative control). Capture and PBS spots are outlined by dashed circles to aid visualization. A 5-parameter logistic fit for the dose-response curve in panel B is shown by the blue curve. Each data point represents the average and the error bars are the standard error of four independent D4 assays. **(E-F)** Optical images and quantification of contact angles on POEGMA and PSBMA polymer brushes. There was statistically signicant differences between group means as determined by Student t-test ($p < 0.001$). Means with lines between bars and marked with a * are significantly different.

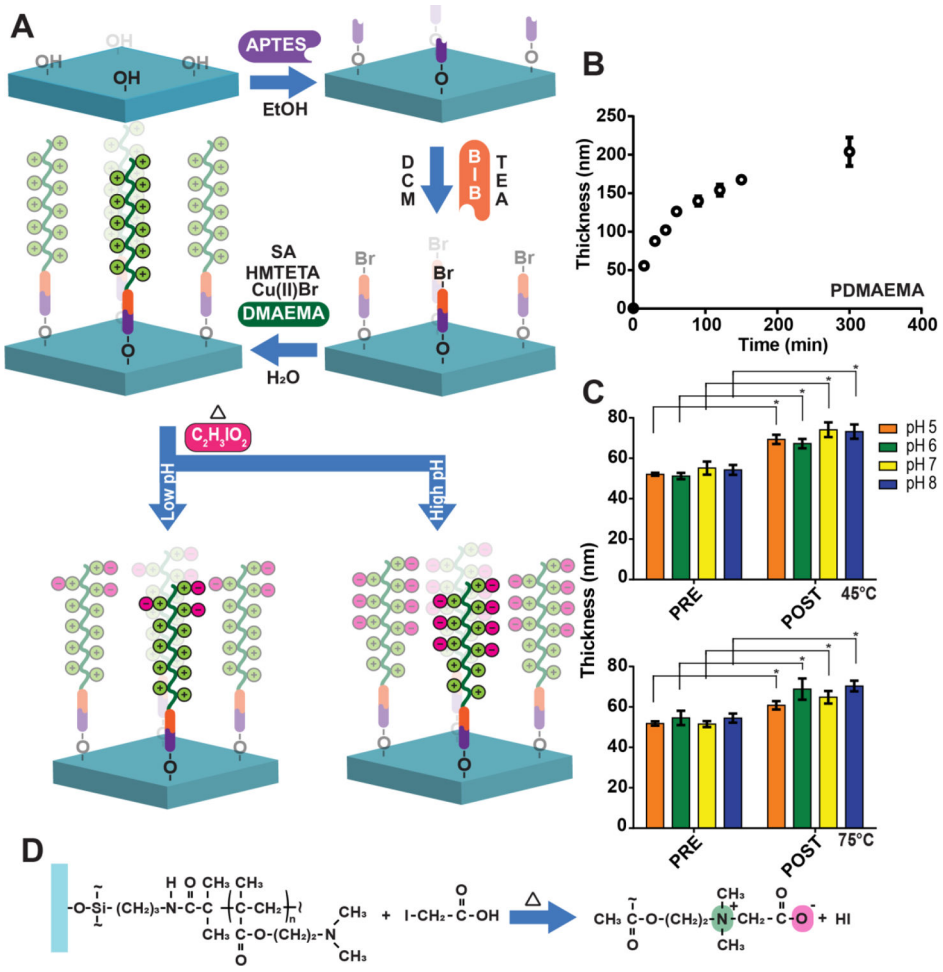

Figure 4: PDMAEMA polymer brushes grown from silicon oxide and glass and their conversion into PCBMA-PDMAEMA hybrid brushes.

(A) Representative stepwise strategy of PCBMA-PDMAEMA hybrid brush synthesis on thermally-deposited SiO_2 on Si and glass slides. Oxide surface functionalization with APTES allows installation of ATRP initiator, BiB (α-bromoisobutyryl bromide). PDMAEMA brushes are then "grafted from" the surface by ATRP and later converted into PCBMA. **(B)** PDMAEMA brush growth on SiO_2 at the indicated timepoints was investigated by reflective mode ellipsometry. **(C)** PDMAEMA brush thickness prior to and post conversion into PCBMA-PDMAEMA under different combinations of pH and temperatures of 45 and 75°C. There was a statistically signicant differences between group means as determined by two-way ANOVA folowed by Sidak's post-hoc test ($p<0.001$). On a pairwise basis, the change in mean thickness post-derivatization compared to the same sample pre-derivitazation was statistically significant for all cases. **(D)** Derivatization reaction of PDMAEMA brush on glass with iodoacetic acid, showing positively and negatively charged groups that form the zwitterionic chemical motif.

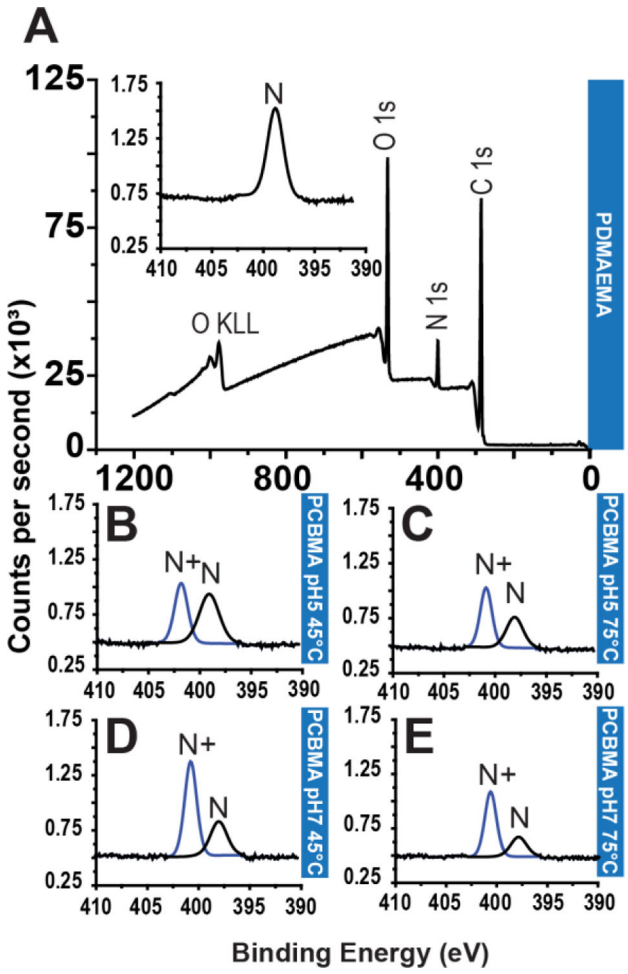

Figure 5: X-ray photoelectron spectra of PDMAEMA and PCBMA-PDMAEMA after derivatization under different conditions.

(A) Survey scan spectrum of PDMAEMA. Inset: High resolution N_{1s} spectrum with peak fitting following SI-ATRP, showing the that the sole nitrogen-containing moity is a tertiary amine, consistent with the structure of PDMAEMA. **(B-E)** High resolution N_{1s} spectra with peak fitting following derivatization under different reaction conditions (B) pH 5 at 45°C, (C) pH 5 at 75°C, (D) pH 7 at 45°C and (E) pH 7 at 75°C, showing the appearance of a second component, that can assigned to a quaternary amine, consistent with the incorporation of a carboxylic acid with a carbon spacer moiety. Survey spectra of PDMAEMA brushes derivatized to PCBMA.

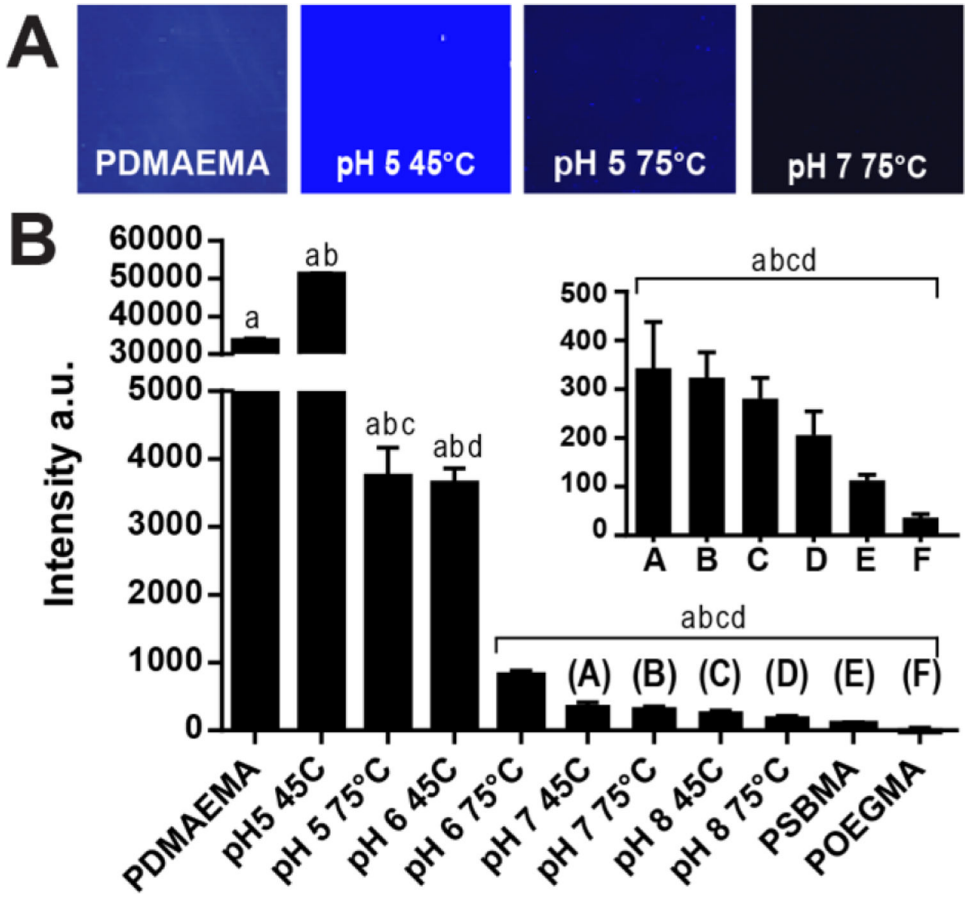

Figure 6: Protein resistance of PDMAEMA and PCBMA-PDMAEMA brushes.

(A-B) Fluorescence images(A) and quantification(B) of protein resistance assays performed with FITC-BSA (10mg/mL in PBS) on PDMAEMA pre- and post-derivatization with iodoacetic acid under different combinations of pH and temperature. There was statisticcally significant difference between group means as determined by one-way ANOVA followed by Tukeys post-hoc test ($p<0.001$).). Means sharing the same letters are significantly different.

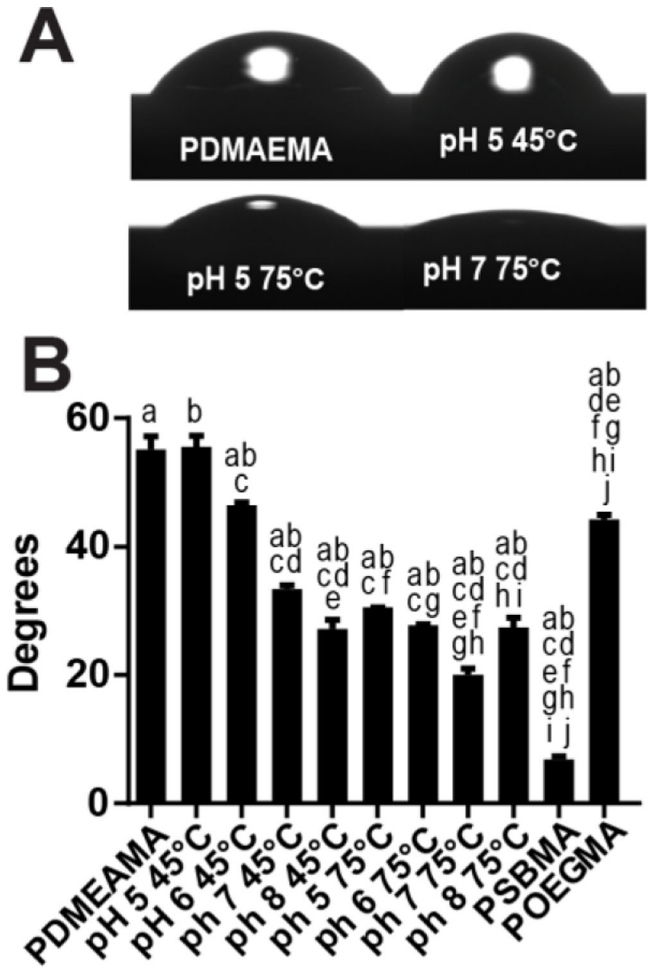

Figure 7: Water contact angle of PDMAEMA and PCBMA-PDMAEMA brushes.

(A-B) Optical images(A) and sessile drop contact angles measurements (B) on PDMAEMA brushes pre- and post-derivatization with iodoacetic acid under different conditions of pH and temperature. There was statistically significant differences between group means as determined by one-way ANOVA folowed by Tukey's post-hoc test ($p<0.001$). Means sharing the same letters are significantly different.

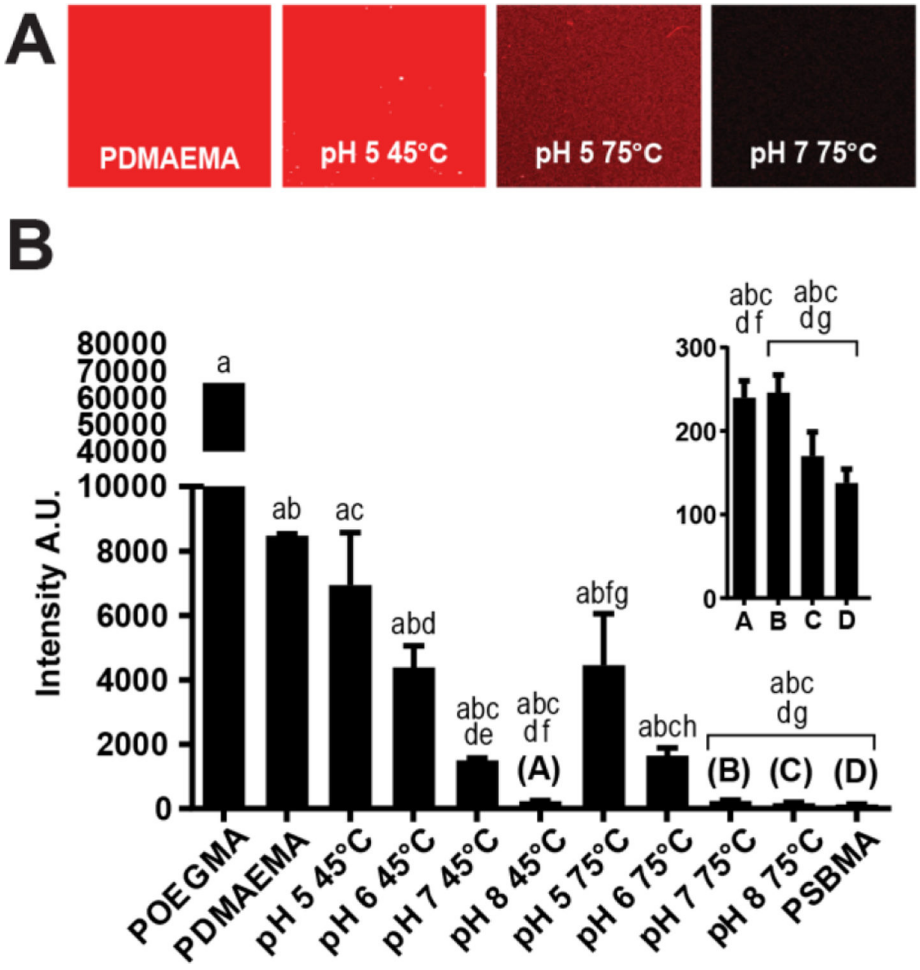

Figure 8: Anti-PEG Ab binding to PDMAEMA and PCBMA-PDMAEMA brushes.

(A-B) Fluorescence images and quantification of anti-PEG Ab resistance assays performed with polyclonal anti-PEG Abs and Alexafluor 647-labeled secondary Abs on PDMAEMA brushes pre- and post-derivatization with iodoacetic acid at different combinations of pH and temperature. There was statistically significant differences between group means as determined by one-way ANOVA ($p<0.001$) folowed by Tukey's post-hoc test. Means sharing the same letters are significantly different.

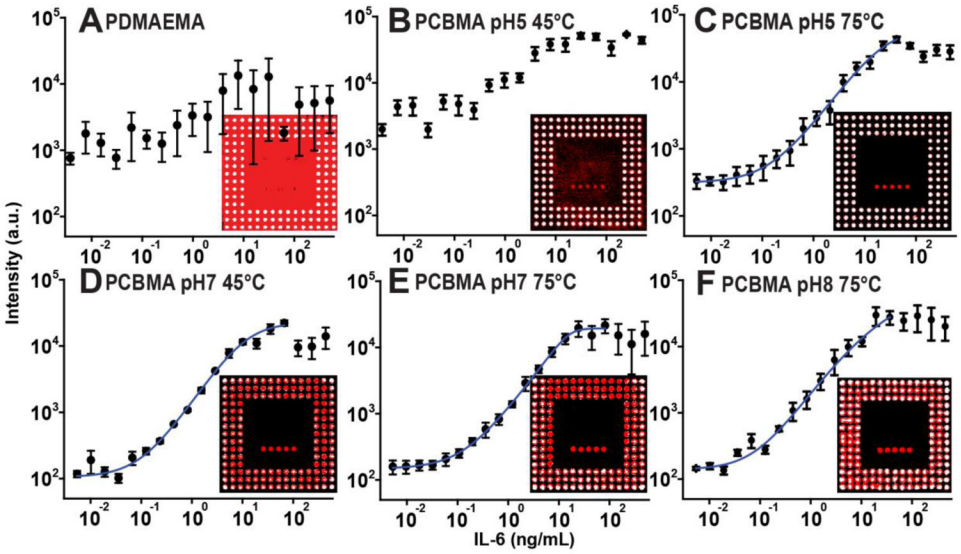

Figure 9: D4 assay dose-response curves.

(A-F) Dose-response curves of D4 assays fabricated on PDMAEMA and PCBMA-PDMAEMA brushes synthesized under different conditions of pH and temperature. Insets depict fluorescence images with detection and capture reagents inkjet printed on the brush coated surfaces. Each point in the dose-response curve is the result of the average and s.e. of three independently conducted D4 assays.A 5-parameter logistic fit is shown by the blue curve.

Table 1:

Atomic concentration of carbon, nitrogen, oxygen and sulfur obtained through survey scans. Tertiary and quaternary amine concentrations obtained with high resolution N 1s scans. Values calculated by peak deconvolution, setting C 1s peak to 284.5 eV, tertiary amine peak to ~398.6 eV and quaternary amine peak to ~402 eV. Abbreviations: N = tertiary amines, N+ = quaternary amines, High Res = High resolution.

		Survey				High Res.	
		C 1s (%)	**N 1s (%)**	**O 1s (%)**	**S 2s (%)**	**N+ (%)**	**N (%)**
	PDMAEMA*	72.7	9.1	18.2	0.0	0.0	100
	PDMAEMA	72.3	6.9	20.8	0.0	0.0	100
	PSBMA*	61.1	5.6	27.8	5.6	100	0.0
	PSBMA	63.0	5.0	26.6	5.4	100	0.0
	PCBMA*	66.7	6.7	26.6	0.0	100	0.0
45°C	PCBMApH5	71.8	6.4	21.8	0.0	44.2	55.8
	PCBMA pH6	70.8	6.1	23.1	0.0	61.7	38.3
	PCBMA pH7	71.0	5.9	23.1	0.0	67.0	33.0
	PCBMA pH8	70.5	5.9	23.6	0.0	62.4	37.6
75°C	PCBMApH5	70.8	6.2	23.0	0.0	57.5	42.5
	PCBMA pH6	71.0	6.0	23.0	0.0	62.5	37.5
	PCBMA pH7	71.0	5.9	23.1	0.0	70.9	29.1
	PCBMA pH8	75.5	5.8	18.7	0.0	60.5	39.5

* The indicated values correspond to the expected stoichiometric percentages of each element

Table 2:

Figures of Merit (LOB, LOD, DR) calculated by averaging 4 independently generated dose-response curves for the detection of IL-6 and surface properties of each substrate given by average water contact angle (WTCA) and protein absorbance levels given by fluorescence level in arbitrary units.

		LOB (pg/mL)	LOD (pg/mL)	DR (log_{10})	WTCA (Degrees)	Prot. Abs Fluorescence
	POEGMA	2	26	3.4	44.3	38
	PSBMA	-	-	-	6.8	113
	PDMAEMA	-	-	-	55.2	33683
45°C	PCBMApH5	-	-	-	55.6	51154
	PCBMApH6	61	81	3.2	46.5	3301
	PCBMA pH7	34	80	2.9	33.4	347
	PCBMA pH8	92	132	2.7	27.2	281
75°C	PCBMA pH5	5	17	4.3	30.5	3469
	PCBMA pH6	11	28	4.3	27.6	872
	PCBMA pH7	12	24	2.7	20.0	324
	PCBMA pH8	18	43	2.4	27.5	205